Simone Giorgetti[1]
Aero-Thermo-Mechanics Department,
Université Libre de Bruxelles,
Avenue Franklin Roosevelt 50,
Brussels 1050, Belgium;
Faculty of Engineering, Université de Mons
(UMONS), Place du Parc 20, Mons 7000,
Belgium,
e-mail: simone.giorgetti@ulb.ac.be

Diederik Coppitters
Thermo and Fluid Dynamics (FLOW),
Vrije Universiteit Brussel,
Rue Fritz Toussaint 8,
Brussels 1050, Belgium

Francesco Contino
Thermo and Fluid Dynamics (FLOW),
Vrije Universiteit Brussel,
Rue Fritz Toussaint 8,
Brussels 1050, Belgium

Ward De Paepe
Faculty of Engineering,
Université de Mons (UMONS),
Place du Parc 20,
Mons 7000, Belgium

Laurent Bricteux
Faculty of Engineering,
Université de Mons (UMONS),
Place du Parc 20,
Mons 7000, Belgium

Gianmarco Aversano
Aero-Thermo-Mechanics Department,
Université Libre de Bruxelles,
Avenue Franklin Roosevelt 50,
Brussels 1050, Belgium

Alessandro Parente
Aero-Thermo-Mechanics Department,
Université Libre de Bruxelles,
Avenue Franklin Roosevelt 50,
Brussels 1050, Belgium

Surrogate-Assisted Modeling and Robust Optimization of a Micro Gas Turbine Plant With Carbon Capture

The growing share of wind and solar power in the total energy mix has caused severe problems in balancing the electrical power production. Consequently, in the future, all fossil fuel-based electricity generation will need to be run on a completely flexible basis. Microgas turbines (mGTs) constitute a mature technology which can offer such flexibility. Even though their greenhouse gas emissions are already very low, stringent carbon reduction targets will require them to be completely carbon neutral: this constraint implies the adoption of postcombustion carbon capture (CC) on these energy systems. Despite this attractive solution, an in-depth study along with a robust optimization of this system has not yet been carried out. Hence, in this paper, a typical mGT with exhaust gas recirculation has been coupled with an amine-based CC plant and simulated using the software ASPEN PLUS. *A rigorous rate-based simulation of the CO_2 absorption and desorption in the CC unit offers an accurate prediction; however, its time complexity and convergence difficulty are severe limitations for a stochastic optimization. Therefore, a surrogate-based optimization approach has been used, which makes use of a Gaussian process regression (GPR) model, trained using the* ASPEN PLUS *data, to quickly find operating points of the plant at a very low computational cost. Using the validated surrogate model, a stochastic optimization has been carried out. As a general result, the analyzed power plant proves to be intrinsically very robust, even when the input variables are affected by strong uncertainties.* [DOI: 10.1115/1.4044491]

Introduction

As a distributed energy technology, microgas turbines (mGTs) offer a great potential for small-scale combined heat and power production, adding flexibility to the electricity system. However, due to the climate change, a very low greenhouse gas emission is a fundamental requirement for our future energy system. On the basis of these considerations, combining an mGT with a carbon capture (CC) plant might offer an effective carbon-clean energy production, but at the cost of an energy penalty. Exhaust gas recirculation (EGR) has recently been proposed as a technological solution which can be applied to the traditional mGT cycle to reduce this CC penalty [1]. EGR consists in injecting back a fraction of the exhaust gas in the compressor inlet to increase the CO_2 content of the working fluid and thus also in the flue gas. Applying this measure, three main advantages can be achieved: lower NO_x emissions, a reduced mass flow rate, and a higher CO_2 concentration of the exhaust gas compared to those of the traditional cycle [2]. However, EGR negatively affects the combustor performance: even though a premixed flame can be sustained at O_2 concentration as low as 14 vol %, the levels of unburned hydrocarbons and CO become already excessively high when the O_2 concentration goes down to 16 vol % [3]. Moreover, EGR has also a slight negative effect on the plant performance due to the higher inlet air temperature of the compressor and the auxiliary energy loss linked to the fan which drives the recirculated gas [4]. Several studies addressing the impact of EGR on GTs and mGTs are available in the literature, showing the advantages and disadvantages of the EGR application [5,6].

[1]Corresponding author.

Manuscript received June 25, 2019; final manuscript received June 26, 2019; published online November 28, 2019. Editor: Jerzy T. Sawicki.

Additional studies focus on the performance of an mGT with both EGR and CC plant: Mansouri et al. used a validated thermodynamic model to show the impact of EGR on Turbec T100 coupled with an amine-based CC unit [7]. Their results demonstrated a considerable improvement compared to the traditional operation. Within this framework, the authors of this paper applied EGR also to the microhumid air turbine and designed the optimal CC unit for both dry and wet operations of the Turbec T100 with EGR [8]. Both the aforementioned studies lean on a deterministic approach to find the optimal operating condition of the plant, taking the parameters of the system as perfectly controllable. Nonetheless, the assumption of deterministic model parameters proves to be inadequate during real-life operation, as the model parameters become subject to uncertainties. Therefore, the considered deterministic design might produce unstable, unforeseen results during its lifetime. To avoid this phenomenon, robust design optimization (RDO) considers uncertainties on the model parameters and provides a design that is less sensitive to the input variations. RDO is applied in numerous domains, such as aerospace, automotive, structural mechanics, and energy systems [9–15]. To find the optimal stochastic design in RDO, genetic algorithm (GA) and its variants are the most applied metaheuristic optimizers due to their widely proven efficiency [16–21]. As in RDO the mean μ_η and the standard deviation σ_η of the electrical efficiency are objectives, the multi-objective variant of GA (nondominated sorting genetic algorithm II (NSGA-II)) is used in this paper.

To acquire these statistical moments for each design sample in a computationally tractable way, a surrogate model is trained based on an experimentally validated ASPEN PLUS model of the mGT with EGR and CC. Surrogate models are mathematical models based on the available data that approximate the underlying hidden relationship between input and output [22]: they are useful when this relationship is either not known or comes in the form of a computationally expensive computer code. Therefore, surrogate models are very popular in uncertainty quantification studies [23–26]. Examples are radial basis functions, polynomial chaos expansion, and Gaussian process regression (GPR). Surrogate models are constructed starting from a relatively small set of *training* observations of the predictive model's output, which correspond to a set of training locations in the model parameter space. GPR was chosen over other regression techniques not only because it provides a distribution for the prediction value, rather than just one value as the prediction, but especially because it allows the user to add prior knowledge on the model by selecting different kernel functions [27].

In this paper, we present a RDO of a typical mGT with EGR and CC unit. The RDO of the system assumes uncertain input variables, which have been considered as Gaussian probability distributions. Using a GPR-based surrogate model, the problem of a harsh time complexity of the rigorous ASPEN PLUS simulation is by-passed. Finally, the NSGA-II solver has been adopted to find the μ_η–σ_η Pareto front or single-point optimum which represent the most robust and most efficient design and operating points of our plant.

Methodology

In the Microgas Turbine With Exhaust Gas Recirculation and Carbon Capture Unit in ASPEN PLUS section of the methodology section, the ASPEN PLUS model of the mGT with EGR and CC is presented. The Gaussian Process Regression-Based Surrogate Model section focuses on the description and training of a GPR surrogate model, based on a restrained dataset of inputs and outputs calculated with the rigorous ASPEN PLUS model. Once the surrogate model has been designed, RDO has been performed by means of a NSGA II optimizer, which is described in the Nondominated Sorting Genetic Algorithm II section.

Microgas Turbine With Exhaust Gas Recirculation and Carbon Capture Unit in ASPEN PLUS. The mGT cycle analyzed in this paper is based on the Turbec T100 mGT [28]. The T100 is, as the majority of mGTs, a recuperated Brayton cycle (Fig. 1). The incoming air is compressed in a centrifugal compressor (1) and thereafter preheated in a recuperator (2) by the flue gas coming from the turbine. The hot air enters the combustion chamber (3), where combustion takes place, burning natural gas. The hot flue gas is expanded in a single-stage centripetal turbine (4). The mechanical power produced by the turbine is partly used to drive the compressor and the remaining part is converted in electrical power using a variable speed generator (5). The thermal energy of the flue gas is first extracted in the recuperator to reduce fuel consumption and, thus, increase the global electrical efficiency. Finally, the remaining thermal energy is traditionally extracted in an economizer (6) in the case of external heat demand, providing hot water at around 70 °C.

The CO_2 concentration of the exhaust gas (1.5 mol % for a traditional mGT cycle) can be enhanced by applying EGR (Fig. 1). EGR is implemented by splitting part of the exhaust gas, cooling it down (7) to maintain a high compression efficiency, separating the condensed water (8), including a blower (9) which drives the requested amount of recirculated gas and, finally, adding a filter (10) to remove possible damaging impurities from the gas.

Subsequently, the exhaust gas coming from the turbine is routed toward a monoethanolamine (MEA)-based CC process (Fig. 1). The exhaust gas enters a cooler (12) to decrease the temperature down to approximately 40 °C. In the absorber (13), cooled flue gas comes into contact with the recycled CO_2-lean MEA aqueous solution and most of the CO_2 (around 90%) is absorbed and thus separated from the flue gas. The CO_2-rich solution, discharged from the absorber, is pumped (14) to the lean/rich heat exchanger (15) where it is preheated by the hot CO_2-lean solution coming from the stripping column (16). In the stripper, the rich solvent is heated up in the reboiler (17) and regenerated.

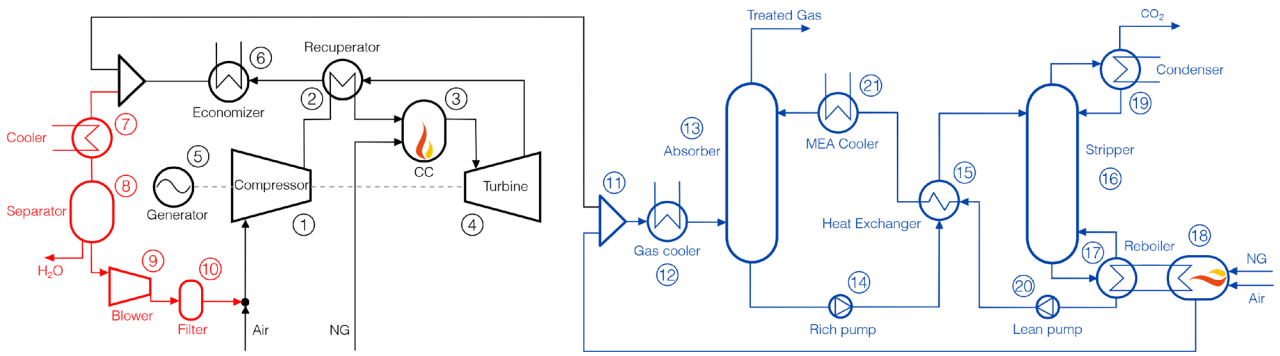

Fig. 1 The Turbec T100 has been modified with EGR and coupled with an amine-based CC for gas treatment

Table 1 List of ASPEN PLUS inputs and outputs with which the GPR surrogate models have been trained

	Inputs			Outputs	
	Variable	Span	Units	Variable	Units
mGT	P_{req}	$70 \div 100$	kW_{el}	$\dot{m}_{ng}$	kg/s
	T_{air}	$10 \div 40$	°C	$\dot{m}_{flue}$	kg/s
	T_{EGR}	$10 \div 40$	°C	Flue gas composition	mol %
	$\%O_2$ (combustor inlet)	$16 \div 18$	%mol	P_{blower}	kW
				T_{mix}	°C
				N	Hz
				$\dot{m}_{air}$	kg/s
				EGR_{ratio}	—
CC	$\dot{m}_{flue}$	mGT model result	kg/s	Reboiler duty	kW
	Flue gas composition	mGT model result	mol %	%MEA of lean solution	mol%
	L/G	$0.9 \div 2$	—	%MEA of rich solution	mol %
	T_{flue}	$35 \div 45$	°C	$\%CO_2$ of lean solution	mol %
	T_{MEA}	$35 \div 45$	°C	$\%CO_2$ of rich solution	mol %
				$\dot{m}_{air,boil}$	kg/s

The regeneration process requires a considerable energy input provided by an external boiler (18), which entails a major energy penalty for the system (around 4 $MJ/kgCO_2$). The CO_2 recovered from the rich solvent leaves from the top of the stripper accompanied by water vapor. That stream is cooled down (19) to condense the water, which is separated and flows back into the stripper. The regenerated lean solvent is discharged from the bottom of the stripper and is pumped (20) first in the lean-rich heat exchanger and is then further cooled down in an air cooler (21).

The mGT cycle, based on the Turbec T100, has been simulated in ASPEN PLUS v10 by adapting the model developed and validated by the authors' research group in Ref. [4]. The original T100 turbomachinery components are included in the model: the actual compressor map is replicated in terms of quasi-dimensionless and corrected parameters (similar compressor maps can be found in Ref. [29]). Due to the variable content of CO_2 and H_2O, the thermodynamic properties of the working fluid will change, which will affect the performance of the compressor. Since the amount of CO_2 in the inlet air remains limited, the compressor map has not been changed (recirculating 60% of the exhaust gas at nominal power output entails a heat capacity change which is less than 0.3%). The turbine is assumed to be choked and to have an isentropic efficiency of 85% (referred to standard air composition). The mechanical efficiency of the turbocomponents is set to 99%. Due to the application of EGR, the turbine choking constant is adjusted by considering the actual gas properties. This has been taken into account by implementing the following equation:

$$\frac{\dot{m}\sqrt{\mathrm{TIT}}}{\mathrm{PIT}} = A\sqrt{\frac{k}{R}\left(\frac{2}{k+1}\right)^{\frac{k+1}{k-1}}} = \text{constant} \tag{1}$$

Analogously, the isentropic efficiency of the turbine has been corrected according to the formula suggested by Parente et al. [30]

$$\frac{\eta}{\eta_*} = \frac{k-1}{k_*-1}\sqrt{\frac{k+1}{k_*+1}\frac{1-1/\pi^{\gamma_*}}{1-1/\pi^{\gamma}}} \quad \text{where} \quad \gamma = \frac{k-1}{k} \tag{2}$$

The combustion chamber has been modeled as a Gibbs reactor with a pressure loss of 5% and a heat loss of 25 kW. The recuperator has been simulated as cross-flow heat exchanger, defining its surface area ($120\,m^2$) and its heat exchange coefficient ($40\,W/m^2\,K$). The property method used to simulate the mGT is the Soave–Redlich–Kwong equation of state.

The CC plant has been modeled and validated against the numerical model of the Pilot-scale advanced capture technology facilities at the UK Carbon Capture and Storage Research Center [31] and described in Ref. [32]. The Electrolyte Non-Random Two Liquid (ELECNRTL) with Perturbed Chain Statistical Associating Fluid Theory (PC-SAFT) equation of state have been used as thermodynamic models. The RadFrac block was used to model both absorber and stripper, and the rate-based MEA model is adopted to provide a rigorous simulation of the two columns. Absorption and desorption physics have been validated against the experimental data found in Refs. [33] and [34]. All the simulations have been performed with a CC rate of 90%. A more in-depth description of the adopted numerical model can be found in Ref. [8]. The natural gas-fired boiler, which provides the reboiler duty for the stripping process, has been simulated as a Gibbs reactor which operates in quasi-stoichiometric conditions (10% of excess air) [35].

Gaussian Process Regression Based Surrogate Model. A rigorous rate-based simulation carried out with ASPEN PLUS offers a very accurate prediction of the physical phenomena which take place in the CC process, but at the cost of a more difficult and time-consuming convergence. From a deterministic point of view, if our objective function is the maximization of the electrical efficiency of the power plant, computational complexity of our rigorous model is still acceptable and ASPEN built-in optimization tool can be used to perform this analysis. In contrast, if our objective function is affected by random influences, such as possible uncertainties related to the input variables, the stochastic behavior of our system makes the time complexity more demanding and often prohibitive. Therefore, a low computational time of the numerical model is a fundamental requirement for this RDO. With this aim in mind, two GPR surrogate models, one for the mGT with EGR and one for the CC unit, have been trained based on a restrained dataset (400 and 1500 operational points, respectively) of inputs and outputs calculated with the rigorous ASPEN PLUS model. The number of training points has been chosen to reduce the relative error between the GPR prediction and the rigorous simulation to a maximum value of 1%. The list of the inputs (with their ranges) and outputs of the two surrogates is shown in Table 1.

For a general output y, every realization $y(\mathbf{x})$ (where $\mathbf{x}$ is an input vector) is expressed in the GPR method as a combination of a trend function and a residual [36]

$$y(\mathbf{x}) = \sum_{i=0}^{p} \beta_i f_i(\mathbf{x}) + z(\mathbf{x}) = \boldsymbol{\beta}^{\mathrm{T}}\mathbf{f}(\mathbf{x}) + z(\mathbf{x}) \tag{3}$$

where the trend function is expressed as a weighted linear combination of $p+1$ polynomials $\mathbf{f}(\mathbf{x}) = [f_0(\mathbf{x}), \ldots, f_p(\mathbf{x})]^{\mathrm{T}}$ with the weights $\boldsymbol{\beta} = [\beta_0, \ldots, \beta_p]^{\mathrm{T}}$ determined by generalized least squares.

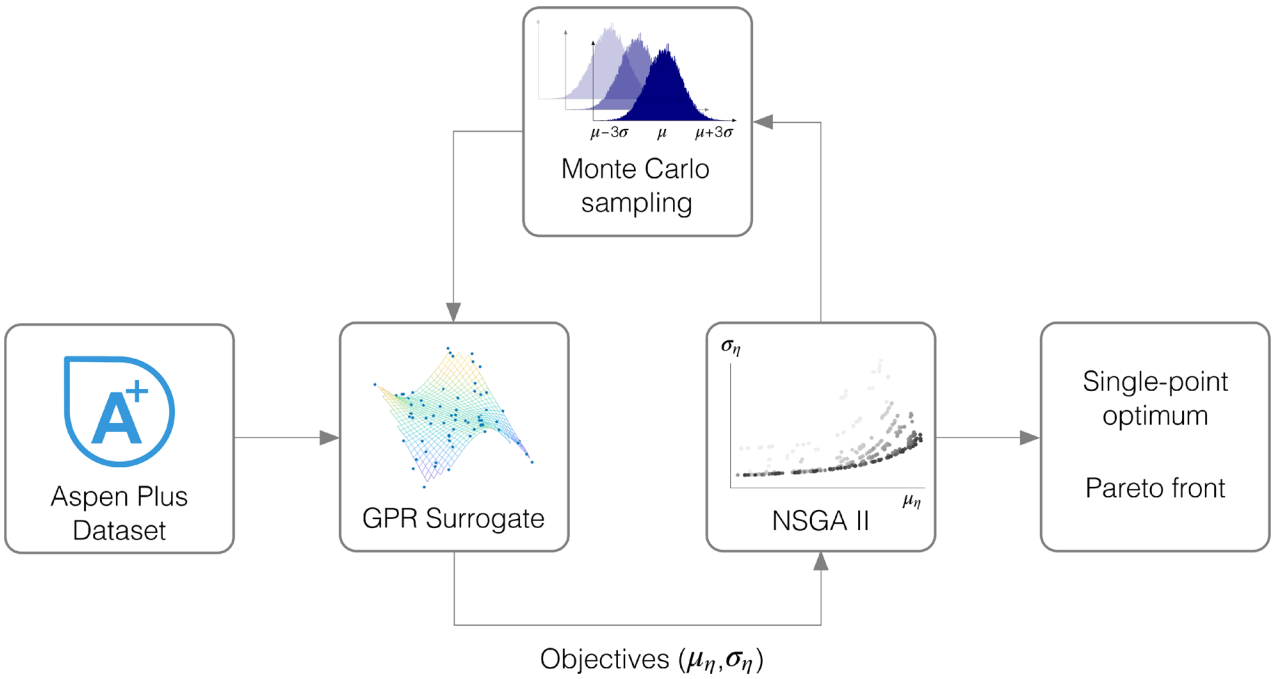

Fig. 2 The ASPEN PLUS-based GPR surrogate calculates our objectives (mean and standard deviation of the plant efficiency) starting from an initial set of uncertain input parameters, considered as Gaussian probability distributions. The NSGA II optimizer infers new input parameters of the GPR model, thus extrapolating a sample evolution toward either an optimal Pareto front or a single-point optimum.

The subscript p also indicates the degree of the polynomial. The residuals $z(\mathbf{x})$ are modeled by a Gaussian process with a kernel or correlation function that depends on a set of hyperparameters to be evaluated by maximum likelihood estimation [36–38]. The time complexity improvement of our numerical model is remarkable, switching from rigorous simulations (order of magnitude of minutes) to surrogate-based simulations which only require several microseconds. Moreover, convergence problems linked to strong nonlinearities and stiffness of the CC model built in ASPEN are by-passed, making the surrogate model robust and reliable.

Nondominated Sorting Genetic Algorithm II. Once the two surrogate models have been trained and validated, they have been used to replace the ASPEN PLUS numerical model in the stochastic optimizations. In this analysis, uncertainties associated with the model input variables are taken into account. Discerning between aleatoric uncertainty (due to the probabilistic variability of our parameters) and epistemic uncertainty (due to limited data and knowledge, thus linked to our numerical model), only the former has been taken into account in this study, assuming that any epistemic uncertainty is subordinate to the aleatoric uncertainty of our input parameters. This is supported by the repeatability (relative error $< \pm 1\%$) of our experimental results used to validate the two numerical models. Therefore, all inputs are assumed as a set of Gaussian probability distributions with mean value μ and standard deviation σ. We have assumed that the associated uncertainty corresponds to a value of 3σ. To calculate the influence of these input uncertainties on the mean value μ_η and standard deviation σ_η of the electrical efficiency, a Monte Carlo sampling has been adopted. To ensure the random sampling independence, the number of random samples has been gradually increased up to a certain value for which any further increment does not affect the value of our objective functions. The optimal sample size has been defined as 50,000 samples for each evaluation. Thereafter, the mean value and the standard deviation of our objective are given to a NSGA II optimization algorithm [17]. The strategy will look for a converged set of design samples whereof every sample dominates every other sample in at least one objective (i.e., Pareto set of solutions). Another study based on this RDO has already been carried out by our research group in Ref. [39]. The NSGA-II algorithm starts from an initial population out of which it creates an offspring based on crossover and mutation rules. The population and offspring samples are sorted based on their dominance in the objectives, where more isolated samples in the design space are favored to ensure an optimal diversification of the set of solutions. This process is repeated until convergence, or the maximum number of generations is reached. In this work, a population count of 24 samples is evaluated over 250 generations. The optimization algorithm is configured with the eta-parameter set at 20, and a crossover and mutation probability of 0.9 and 0.1, respectively. A schematic overview of the RDO procedure is represented in Fig. 2.

Results

In this section, numerical results of the RDO are discussed: first, a comparison between the most robust solution and the most efficient solution varying the input uncertainties is presented. Subsequently, the σ–μ optimal operational points with fixed requested electrical power outputs are shown. Finally, a sensitivity analysis assuming different fixed T_{air} and T_{EGR} is performed which shows the Pareto front evolution as a function of T_{air}.

Uncertainty Influence of the Input Parameters. To characterize the robustness of our model, a preliminary analysis varying the input uncertainties has been carried out. Two different scenarios have been taken into account: a first case where actual uncertainties have been considered (realistic uncertainties) and a second case in which the input uncertainties have been overestimated (precautionary uncertainties). The realistic uncertainties are based on actual measurement errors of our inputs, while the precautionary uncertainties are calculated assuming a low-quality measurement. The two different cases are shown in Table 2.

For both scenarios, no fixed input has been set, namely, all inputs parameters have been allowed to vary along their whole span (as defined in Table 1). The result of the robust analysis is

Table 2 Two scenarios considering different input uncertainties are considered to analyze the robustness of our plant

	Inputs	Units	Realistic uncertainties	Precautionary uncertainties
mGT	P_{req}	kW_{el}	±1 kW	±1 kW
	T_{air}	°C	±1 °C	±2 °C
	T_{EGR}	°C	±1 °C	±2 °C
	$\%O_2$	mol %	±2% (relative)	±4% (relative)
CC	L/G	—	±7%	±10%
	T_{flue}	°C	±1 °C	±2 °C
	T_{MEA}	°C	±1 °C	±2 °C

depicted in Fig. 3. Two different Pareto fronts μ_η–σ_η are obtained. Independently from the envisaged scenario, the standard deviation σ_η shows a restrained span of values between the most robust and the most efficient (but less robust) solution. As expected, the values of the standard deviation in the precautionary uncertainties scenario are greater than that of the realistic case. Nevertheless, in both cases, the fluctuation of the mean value has a very minor effect: the coefficient of variation defined as σ_η/μ_η is always lower than 0.12% for the low uncertainty case and 0.25% for the high uncertainty scenario. This means that our system is intrinsically very robust, even when our input variables are affected by strong uncertainties. As a result, although a most robust operating point has been found, it is always more convenient to work close to the most efficient point. It is important to note that both optimal points of the two Pareto fronts are coherent to the deterministic solution. The only difference is due to the presence of input uncertainties which shift the optimal solution to avoid operating points out of their boundaries, such as the minimum level of oxygen. The final stochastic solutions together with the deterministic one are represented in Table 3. For the following studies of this paper, only the realistic uncertainties are considered.

Different Requested Power Scenarios. The first sensitivity analysis is based on different requested electrical power outputs P_{req}. For each power output, constant values of T_{air} and T_{EGR} of, respectively, 15 °C and 25 °C have been assumed. Therefore, the only parameters which can vary are the concentration of oxygen in combustor inlet (set by the EGR_{ratio}), the L/G ratio, the flue gas cooling temperature T_{flue}, and the MEA cooling temperature T_{MEA}. Nevertheless, each parameter is assumed uncertain (realistic uncertainties in Table 2 are assumed), independently from being fixed or variable. Four optimization routines have been performed considering operating conditions of 70, 80, 90, and 100 kW_{el}.

As shown in Fig. 4(*a*), the optimal stochastic solutions are not Pareto fronts but single-point optimums. This is strictly linked to the fixed requested power output constraint. It is important to note that the standard deviation range is very similar to the one shown in figure in the case of low uncertainty case. As previously described, the small standard deviation associated with each P_{req} demonstrates the robustness of the plant, maintaining an optimal electrical efficiency close to the one obtained with a deterministic approach. Analyzing the input parameters which correspond to these optimal values of μ_η, it is interesting to notice the increasing trend of oxygen content, namely, decreasing the EGR_{ratio} of the mGT, when operating in part load (Fig. 4(*b*)). This result goes against the deterministic idea of keeping the highest EGR_{ratio} to make the CC process less intensive. This phenomenon can be explained as follows: decreasing the EGR_{ratio}, the energy demand

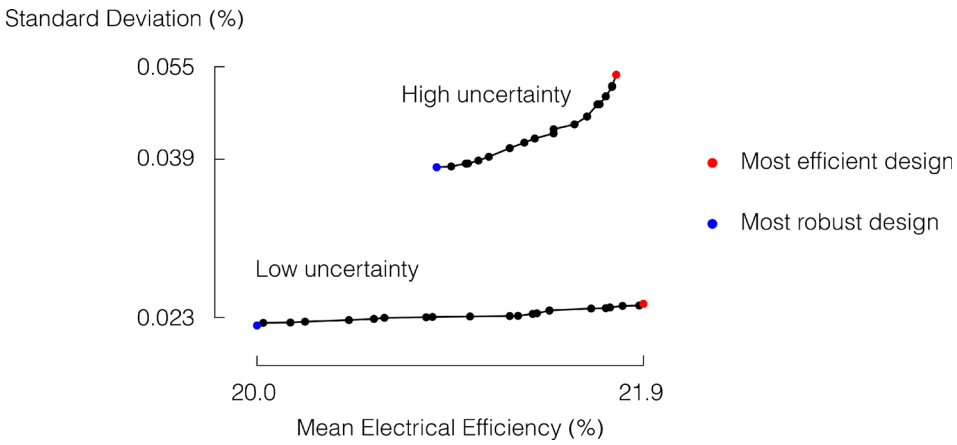

Fig. 3 Although the Pareto fronts involve a remarkable variation of the electrical efficiency, its standard deviation has a negligible influence. Therefore, the most optimal solution, even though slightly less robust, can be assumed as the most advantageous solution.

Table 3 The most efficient (but least robust) stochastic solutions, extrapolated from the Pareto front, are very similar to the deterministic one

	Inputs	Units	Realistic uncertainties	Precautionary uncertainties	Deterministic solution
mGT	P_{req}	kW_{el}	99	99	100
	T_{air}	°C	11	12	10
	T_{EGR}	°C	11	12	10
	$\%O_2$	mol %	16.3	16.7	16.0
CC	L/G	—	1.3	1.25	1.35
	T_{flue}	°C	37	37	35
	T_{MEA}	°C	44	42	45
Electrical efficiency	μ_η	%	21.9	21.8	22.1

Note: The slight difference is due to uncertainties which shift the optimal solution to avoid operating points out of their boundaries.

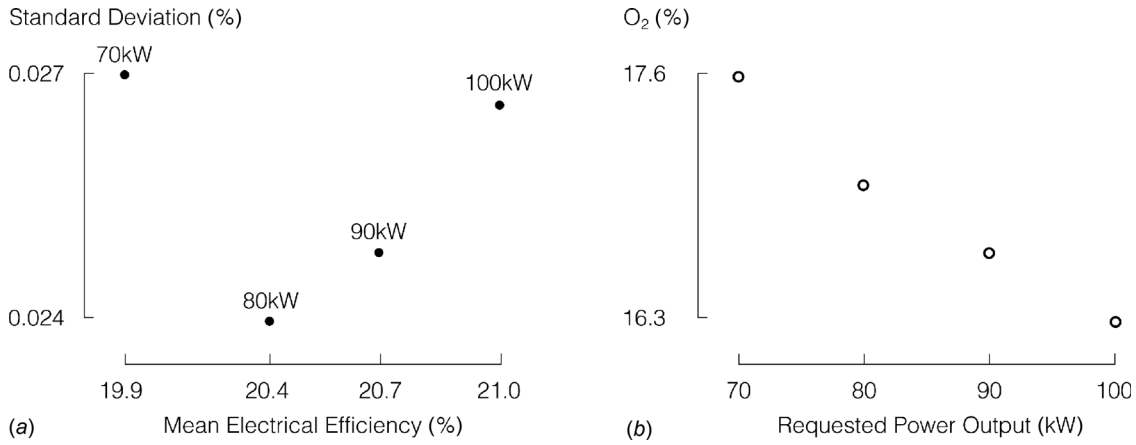

Fig. 4 Operating at a requested power output of 80 kW is the most robust operation (*a*). From a RDO point of view, the O_2 concentration is not kept to a minimum value of 16% (limit value for an efficient combustion) but it increases when working in part load conditions (*b*). This is beneficial for the robustness of the plant and it does not influence the maximal electrical efficiency.

of the EGR blower decreases, but the CO_2 content and the mass flow rate of flue gas increase, making the CC more inefficient. However, it must be considered that the CC plant has been designed for nominal conditions of the mGT, therefore, when the mGT is working in part load, the flue gas mass flow rate is lower (at 70 kW, its value is around the half of that at 100 kW) and the CC process is more efficient since oversized for this rate. The EGR_{ratio} can be reduced entailing an electrical efficiency which is approximately the same as the one of the deterministic solution (which always sets the $\%O_2$ content equal to 16%) but with a gain in robustness.

Sensitivity Analysis Changing Inlet Air Temperature. As a last step, a sensitivity study varying the air inlet temperature and the EGR cooling temperature is performed. In this analysis, fixed values of T_{air} and T_{EGR} have been assumed, with the constraint $T_{EGR} = T_{air} + 10\,^{\circ}C$ (traditional air cooled heat exchanger). All the other inputs have been allowed to vary along their validity ranges. In these conditions, a family of Pareto fronts is obtained as shown in Fig. 5.

The most efficient solutions for each T_{air} scenario are obtained at maximal request power output and maximal MEA cooling temperature (respectively, 99 kW and 44 °C) and at minimal $\%O_2$ concentration in the combustor inlet (therefore maximal EGR_{ratio}) and minimal flue gas cooling temperature (respectively, 16.3% and 36 °C). In these conditions, the optimal *L*/*G* ratio of the CC plant is 1.3 for all cases (close to the deterministic optimal *L*/*G* ratio of 1.35). These results are coherent with the correspondent deterministic solutions of the plant. It can also be noticed how the standard deviation of the most efficient solution tends to increase when increasing the T_{air} temperature. Hence, increasing the air inlet temperature has a negative impact not only on the efficiency of the plant but also on its standard deviation, thus its robustness. Finally, the most robust solution for each T_{air} scenario is achieved when working with an requested power output of 80 kW (which is coherent with the result obtained in Fig. 4), with an O_2 content of 16.8%, *L*/*G* ratio of 1.25, and both T_{flue} and T_{MEA} of around 42 °C.

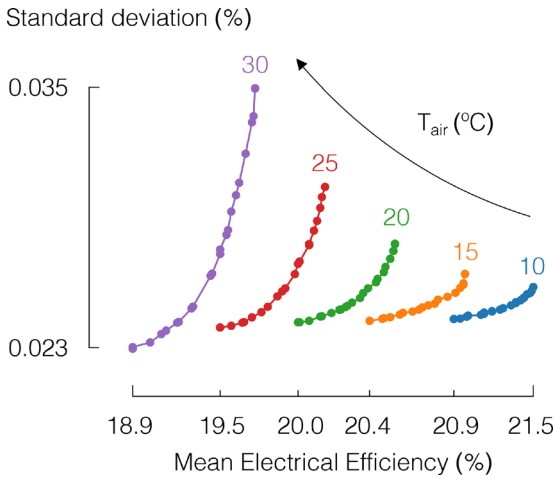

Fig. 5 Increasing the T_{air} (and accordingly T_{EGR}), the electrical efficiency of the plant diminishes while its standard deviation increases, making the power plant operation not only less efficient but also less robust

Conclusions

In this paper, a RDO of a typical mGT with EGR and CC unit is presented. The analysis has been performed on a GPR-based surrogate model trained on a rigorous ASPEN PLUS dataset. In this way, a remarkable improvement on time complexity and numerical stability of the calculation has been achieved. By means of the multi-objective solver NSGA-II, optimal operating points and Pareto fronts of μ_η–σ_η have been found and discussed. For each analysis, the standard deviation σ_η of the electrical efficiency has a very limited span and does not have a significant weight on the electrical efficiency μ_η. This demonstrates the strong robustness of our power plant when introducing model input fluctuations. The RDO allowed us to find more reliable operating conditions of the plant: in the case of fixed requested power output, the stochastic optimal solution is not achieved for the maximum EGR_{ratio} (as in the case of deterministic optimal solution), but its value decreases when working in part load. Moreover, a sensitivity analysis varying T_{air} and T_{EGR} has been carried out, showing a more detailed result compared to a deterministic approach: the increasing temperature does not only involve a decreasing mean electrical efficiency of the plant but also involve a less robust condition when working in the most efficient condition.

Perspectives

In the future work, we will introduce a multi-objective approach in which different targets are put forward, such as maximum electrical power output, maximum electrical efficiency, and maximum global (electrical + thermal) efficiency considering also energy integration between the CC unit and the mGT to achieve the optimal and the most robust operating condition of the plant for each energy scenario.

Acknowledgment

The authors would like to acknowledge "Flexible eneRgy vEctors of the futurE (FREE) project," supported by ENGIE. The first author acknowledges the support of Funds pour la Recherche Scientifique (FNRS) through a FRIA fellowship for the project CONCERT: CarbON CapturE Ready gas Turbine.

Funding Data

- Funds pour la Recherche Scientifique (FNRS) (FRIA fellowship; Funder ID: 10.13039/501100002661).

Nomenclature

Symbols

A = choking coefficient
f = GPR polynomial function
k = heat capacity ratio
$\dot{m}$ = mass flow rate
N = shaft speed
P = power output
R = gas constant
T = temperature
x = GPR training sample
y = GPR prediction
z = GPR residual
β = GPR weight
η = electrical efficiency
μ = mean value
π = pressure ratio
σ = standard deviation

Subscripts

air = air
blower = external boiler
boil = external boiler
EGR = exhaust gas recirculation stream
flue = flue gas
MEA = monoethanolamine
mix = mixing (mGT and boiler flue gases)
ng = natural gas
ratio = EGR—total flue gas volumetric ratio
req = requested
η = electrical efficiency

Superscript

* = referred to standard air composition

Acronyms

CC = carbon capture
EGR = exhaust gas recirculation
GA = genetic algorithm
GPR = Gaussian process regression
L/G = liquid(monoethanolamine)–gas(flue gas) ratio
MEA = monoethanolamine
mGT = microgas turbine
NSGA II = nondominated Sorting genetic algorithm II
PIT = turbine inlet pressure
RDO = robust design optimization
TIT = turbine inlet temperature

References

[1] González-Salazar, M. A., 2015, "Recent Developments in Carbon Dioxide Capture Technologies for Gas Turbine Power Generation," Int. J. Greenhouse Gas Control, **34**, pp. 106–116.
[2] ElKady, A. M., Evulet, A., Brand, A., Ursin, T. P., and Lynghjem, A., 2009, "Application of Exhaust Gas Recirculation in a DLN F-Class Combustion System for Postcombustion Carbon Capture," ASME J. Eng. Gas Turbines Power, **131**(3), p. 034505.
[3] Ditaranto, M., Hals, J., and Bjørge, T., 2009, "Investigation on the In-Flame NO Reburning in Turbine Exhaust Gas," Proc. Combust. Inst., **32**(2), pp. 2659–2666.
[4] De Paepe, W., Giorgetti, S., Montero Carrero, M., Bram, S., and Contino, F., 2016, "Exhaust Gas Recirculation on Humidified Flexible Micro Gas Turbines for Carbon Capture Applications," ASME Paper No. GT2016-57265.
[5] Li, H., Ditaranto, M., and Berstad, D., 2011, "Technologies for Increasing CO_2 Concentration in Exhaust Gas From Natural Gas-Fired Power Production With Post-Combustion, Amine-Based CO_2 Capture," Energy, **36**(2), pp. 1124–1133.
[6] Alcaráz-Calderon, A. M., González-Díaz, M. O., Mendez, Á., González-Santaló, J. M., and González-Díaz, A., 2017, "Natural Gas Combined Cycle With Exhaust Gas Recirculation and CO_2 Capture at Part-Load Operation," J. Energy Inst., **92**(2), pp. 370–381.
[7] Majoumerd, M. M., Nikpey Somehsaraei, H., Assadi, M., and Breuhaus, P., 2014, "Micro Gas Turbine Configurations With Carbon Capture—Performance Assessment Using a Validated Thermodynamic Model," Appl. Therm. Eng., **73**(1), pp. 172–184.
[8] Giorgetti, S., Bricteux, L., Parente, A., Blondeau, J., Contino, F., and Paepe, W. D., 2017, "Carbon Capture on Micro Gas Turbine Cycles: Assessment of the Performance on Dry and Wet Operations," Appl. Energy, **207**, pp. 243–253.
[9] Chatterjee, T., Chakraborty, S., and Chowdhury, R., 2017, "A Critical Review of Surrogate Assisted Robust Design Optimization," Arch. Comput. Methods Eng., **26**(1), pp. 245–274
[10] Parisio, A., Del Vecchio, C., and Vaccaro, A., 2012, "A Robust Optimization Approach to Energy Hub Management," Int. J. Electr. Power Energy Syst., **42**(1), pp. 98–104.
[11] Cheng, J., Liu, Z., Wu, Z., Li, X., and Tan, J., 2015, "Robust Optimization of Structural Dynamic Characteristics Based on Adaptive Kriging Model and CNSGA," Struct. Multidiscip. Optim., **51**(2), p. 423.
[12] Kamjoo, A., Maheri, A., Dizqah, A., and Putrus, G., 2015, "Multi-Objective Design Under Uncertainties of Hybrid Renewable Energy System Using NSGA-II and Chance Constrained Programming," Int. J. Electr. Power Energy Syst., **74**, pp. 187–194.
[13] Kuznetsova, E., Ruiz, C., Li, Y.-F., and Zio, E., 2015, "Analysis of Robust Optimization for Decentralized Microgrid Energy Management Under Uncertainty," Int. J. Electr. Power Energy Syst., **64**, pp. 815–832.
[14] Majewski, D. E., Wirtz, M., Lampe, M., and Bardow, A., 2017, "Robust Multi-Objective Optimization for Sustainable Design of Distributed Energy Supply Systems," Comput. Chem. Eng., **102**, pp. 26–39.
[15] Akbari, K., Nasiri, M., Jolai, F., and Ghaderi, S., 2014, "Optimal Investment and Unit Sizing of Distributed Energy Systemsunder Uncertainty: A Robust Optimization Approach," Energy Build., **85**, p. 275.
[16] Gaspar-Cunha, A., and Covas, J. A., 2006, "Robustness Using Multi-Objective Evolutionary Algorithms," Arch. Comput. Methods Eng., **36**, pp. 353–362.
[17] Deb, K., Pratap, A., Agarwal, S., and Meyarivan, T., 2002, "A Fast and Elitist Multiobjective Genetic Algorithm: NSGA-II," IEEE Trans. Evol. Comput., **6**(2), pp. 182–197.
[18] Saha, A., and Ray, T., 2011, "Practical Robust Design Optimization Using Evolutionary Algorithms," ASME J. Mech. Des., **133**(10), p. 101012.
[19] Tsirikoglou, P., Abraham, S., Contino, F., Bağci, O., Vierendeels, J., and Ghorbaniasl, G., 2017, "Comparison of Metaheuristics Algorithms on Robust Design Optimization of a Plain-Fin-Tube Heat Exchanger," AIAA Paper No. 2017–3827.
[20] Tsirikoglou, P., Abraham, S., Contino, F., Lacor, C., and Ghorbaniasl, G., 2017, "A Hyperparameters Selection Technique for Support Vector Regression Models," Appl. Soft Comput., **61**, pp. 139–148.
[21] Abraham, S., Tsirikoglou, P., Miranda, J., Lacor, C., Contino, F., and Ghorbaniasl, G., 2018, "Spectral Representation of Stochastic Field Data Using Sparse Polynomial Chaos Expansions," J. Comput. Phys., **367**, pp. 109–120.
[22] Aversano, G., Parra-Alvarez, J. C., Isaac, B. J., Smith, S. T., Coussement, A., Gicquel, O., and Parente, A., 2018, "PCA and Kriging for the Efficient Exploration of Consistency Regions in Uncertainty Quantification," Proc. Combust. Inst., **37**(4), pp. 4461–4469.
[23] Owen, N. E., Challenor, P., Menon, P. P., and Bennani, S., 2015, "Comparison of Surrogate-Based Uncertainty Quantification Methods for Computationally Expensive Simulators," SIAM/ASA Uncertainty Quantification, **5**(1), pp. 403–435.
[24] De Lozzo, M., and Marrel, A., 2017, "Sensitivity Analysis With Dependence and Variance-Based Measures for Spatio-Temporal Numerical Simulators," Stochastic Environ. Res. Risk Assess., **31**(6), pp. 1437–1453.
[25] Dubreuil, S., Berveiller, M., Petitjean, F., and Salaün, M., 2014, "Construction of Bootstrap Confidence Intervals on Sensitivity Indices Computed by Polynomial Chaos Expansion," Reliab. Eng. Syst. Saf., **121**, pp. 263–275.
[26] Marrel, A., Iooss, B., Laurent, B., and Roustant, O., 2009, "Calculations of Sobol Indices for the Gaussian Process Metamodel," Reliab. Eng. Syst. Saf., **94**(3), pp. 742–751.
[27] Rasmussen, C. E., and Williams, C., 2006, *Gaussian Processes for Machine Learning*, The MIT Press, Cambridge, MA.
[28] Turbec, A. B., 2000, "T100 Microturbine CHP System: Technical Description Ver 4.0, (2000–2001)".
[29] Caresana, F., Pelagalli, L., Comodi, G., and Renzi, M., 2014, "Microturbogas Cogeneration Systems for Distributed Generation: Effects of Ambient Temperature on Global Performance and Components' Behavior," Appl. Energy, **124**, pp. 17–27.

[30] Parente, J., Traverso, A., and Massardo, A. F., 2003, "Micro Humid Air Cycle—Part A: Thermodynamic and Technical Aspects," ASME Paper No. GT2003-38326.
[31] Pilot-Scale Advanced Capture Technology, 2018, "Pilot-Scale Advanced Capture Technology," accessed Oct. 28, 2018, https://pact.group.shef.ac.uk/facilities/
[32] Agbonghae, E. O., Best, T., Finney, K. N., Palma, C. F., Hughes, K. J., and Pourkashanian, M., 2014, "Experimental and Process Modelling Study of Integration of a Micro-Turbine With an Amine Plant," Energy Procedia, **63**, pp. 1064–1073.
[33] Zhang, Y., Que, H., and Chen, C.-C., 2011, "Thermodynamic Modeling for CO_2 Absorption in Aqueous MEA Solution With Electrolyte NRTL Model," Fluid Phase Equilib., **311**, pp. 67–75.
[34] Zhang, Y., Que, H., and Chen, C.-C., 2011, "Thermodynamic Modeling for CO_2 Absorption in Aqueous MDEA Solution With Electrolyte NRTL Model," Ind. Eng. Chem. Res., **50**, pp. 163–175.
[35] Baukal, C. E., Jr., 2001, *The John Zink Combustion Handbook*, John Zink Company LLC, CRC press, New York.
[36] Constantine, P. G., Dow, E., and Wang, Q., 2014, "Active Subspace Methods in Theory and Practice," SIAM J. Sci. Comput., **36**(4), pp. 1500–1524.
[37] Lophaven, S. N., Søndergaard, J., and Nielsen, H. B., 2002, "Kriging Toolbox" .
[38] Seeger, M., 2004, *Gaussian Processes for Machine Learning*, Int. J. Neural Syst., Vol. 14, pp. 69–106.
[39] De Paepe, W., Coppitters, D., Abraham, S., Tsirikoglou, P., Ghorbaniasl, G., and Contino, F., 2019, "Robust Operational Optimization of a Typical Micro Gas Turbine," Energy Procedia., **158**, pp. 5795–5803.